Wei Jia (Orcid ID: 0000-0002-5879-3870)
Han Tongcheng (Orcid ID: 0000-0003-1009-3629)
Carcione José, M (Orcid ID: 0000-0002-2839-705X)

Thermoelastic dispersion and attenuation of P- and SV-wave scattering by aligned fluid-saturated cracks of finite thickness in an isothermal elastic medium

Jia Wei[1,5,6], Li-Yun Fu[2,3]*, Tongcheng Han[3] and José M. Carcione[4]

1 Key Laboratory of Petroleum Resource Research, Institute of Geology and Geophysics, Chinese Academy of Sciences, 19 Beitucheng Western Road, Chaoyang District, Beijing 100029, China

2 Laboratory for Marine Mineral Resources, Qingdao National Laboratory for Marine Science and Technology, Qingdao 266071, China

3 Key Laboratory of Deep Oil and Gas, China University of Petroleum (East China), 66 Changjiang West Road, Huangdao District, Qingdao 266580, China

4 National Institute of Oceanography and Applied Geophysics (OGS), Trieste, Italy

5 University of Chinese Academy of Sciences, 19(A) Yuquan Road, Shijingshan District, Beijing 100049, China

6 Innovation Academy for Earth Science, Chinese Academy of Sciences, 19 Beitucheng Western Road, Chaoyang District, Beijing 100029, China

*Corresponding author: lfu@upc.edu.cn

This article has been accepted for publication and undergone full peer review but has not been through the copyediting, typesetting, pagination and proofreading process which may lead to differences between this version and the Version of Record. Please cite this article as doi: 10.1029/2020JB019942

Key Points:

- We study the thermoelastic dispersion and attenuation of P- and SV-wave scattering by aligned-crack in an isothermal elastic medium;
- The dissipation increases with increasing temperature, but the scattering is inhibited at a given temperature;
- The P wave shows a strong sensitivity to temperature along the crack normal, whereas the SV wave behaves in opposite manner.

Abstract

P- and SV-wave scattering by thermally-constrained saturated cracks couples elastic deformation with temperature. We estimate the scattering attenuation and velocity dispersion by aligned fluid-saturated cracks with finite thickness, which are sparsely and randomly embedded in an isothermal and isotropic elastic medium. By incorporating thermoelastic effects into the representation theorem with the non-interaction Foldy approximation, we formulate the dispersion and attenuation of P and SV waves induced by displacement discontinuities across aligned cracks constrained by a thermoelastic boundary condition. The frequency-dependent response as a function of temperature is calculated for various P- and SV-wave incidence angles. The resulting scattering attenuation and dispersion are compared with those of the conventional aligned-crack model. The examples show that the dissipation increases with increasing temperature, but the scattering is inhibited at a given temperature. The P wave shows a strong sensitivity to temperature along the direction normal to the cracks, whereas the SV wave has an opposite behavior. This theory has the potential to assess the

distribution of temperature from seismic attributes.

1 Introduction

The Earth can be modelled as an inhomogeneous thermoelastic medium, in which wave propagating suffers frequency-dependent energy losses (Treitel, 1959). Thermoelasticity has been recognized as a feasible mechanism for intrinsic dissipation in the lithosphere (Aki, 1980; Sato *et al*., 2012). Seismic dispersion and attenuation in dry and saturated cracked rocks have been extensively investigated in many disciplines. Savage (1966) studies the thermoelastic attenuation of elastic waves caused by empty elliptical cracks. Other early works (e.g., Mal 1970a, 1970b; Martin 1981; Krenk and Schmidt 1982) address the scattering process by a single dry crack in an infinite isotropic elastic solid. The scattering effect of multiple dry cracks (e.g., Kikuchi, 1981; Zhang and Achenbach, 1991; Kawahara, 1992; Zhang and Gross, 1993a, 1993b) can naturally be described with the non-interaction Foldy approximation (Foldy, 1945) for cracks distributed sparsely and randomly in an elastic solid. These models are extended to wave scattering by aligned fluid-saturated cracks including viscous fluids (Kawahara and Yamashita 1992), the effect of finite thickness (Guo *et al.* 2018c; Song *et al.*, 2020a, 2020b), the mechanism of hydraulic conduction (Song *et al.*, 2019), and the wave-induced fluid flow attenuation of porous media (e.g., Galvin & Gurevich, 2006, 2007, 2009; Guo *et al.*, 2018a, 2018b; Phurkhao, 2013; Song *et al.*, 2017; Fu *et al.*, 2018, 2020).

Thermoelasticity couples elastic deformations with temperature, based on the thermodynamics of irreversible processes (Biot, 1956; Deresiewicz, 1957). Temperature fluctuations result in thermal stress and wave dissipation. This mechanism is relevant to geophysical and geothermal exploration (e.g., Armstrong, 1984; Cermak *et al.*, 1990; Fu, 2012, 2017; Jacquey *et al.* 2015; Poletto e*t al.*, 2018), and earthquake seismology (e.g., Boschi, 1973; Simmons *et al.*, 2010; Ritsema *et al.*, 2011). The classical theory of thermoelasticity is based on a parabolic-type heat-transfer equation, causing unphysical solutions such as infinite velocities as a function of frequency. More general equations by analogy with the Maxwell model of viscoelasticity avoid this unphysical behavior by introducing relaxation-time terms into the heat equation, e.g., the Lord-Shulman thermoelasticity equations (Lord and Shulman, 1967; Green and Lindsay, 1972; Eslami *et al*., 2013). Based on the Lord-Shulman theory, Rudgers (1990) analyzes the physics of thermoelastic wave propagation, Carcione *et al.* (2018) computes synthetic seismograms and Wang *et al.* (2019) obtain the corresponding Green function. Moreover, Carcione *et al*. (2019) generalize these thermoelastic equations to the poroelastic case. Recently, Wei *et al*. (2020) derive the frequency-domain Green function of the Lord-Shulman thermo-poroelasticity theory.

In the present work, we incorporate the thermoelasticity theory to describe the elastic deformation of non-viscous fluid-saturated cracks to analyze the effects on wave scattering. We study the seismic dispersion and attenuation as a function of temperature and wave incident angle. The model is based on 2D aligned fluid-saturated cracks distributed sparsely and randomly in an isothermal and isotropic elastic medium. The theory is based on the representation theorem with the non-interaction Foldy approximation, and we formulate the dispersion and attenuation of P and SV waves induced by displacement discontinuities across the cracks constrained by the thermoelastic boundary condition.

2 Formulation of the boundary-value problem

We consider a model of thermoelastic cracks, modified from the P-wave scattering model of Guo *et al.* (2018c) for fluid-saturated cracks, which in turn is developed from that of

Kawahara (1992) for dry open slit cracks with finite thickness. As shown in Figure 1, the 2D aligned cracks are randomly and homogeneously distributed through an infinite, isothermal and isotropic elastic (non-porous) background medium. The crack density ν, defined as the number of cracks per unit area, is assumed to be sufficiently small. All the cracks having the same rectangular shape, with thickness h and length $2a$, are assumed to be parallel to the X_1-axis but infinitely long along the X_3-axis to satisfy the plane-strain condition in the X_1–X_2 plane. Hence, the 3D problem can be reduced to a 2D problem. We consider an incident harmonic plane P (or SV) wave of angular frequency ω at an angle φ (or ϕ) measured from the crack normal (X_2-axis). Two mechanisms are involved: wave scattering and thermoelastic dissipation by thermal loading through crack boundaries. The thermoelastic boundary conditions are introduced in this section, providing the basis to formulate the model for aligned fluid saturated thermoelastic cracks.

2.1 Thermoelastic boundary conditions

The aligned cracks are subject to thermoelastic boundary conditions associated with the isothermal background medium. The constitutive relations of thermoelasticity for the stress components σ_{ij} can be expressed as (Biot, 1956; Carcione *et al.*, 2020)

$$\sigma_{ij} = \lambda\delta_{ij}\theta + \mu u_{i,j} + \mu u_{j,i} - \beta\delta_{ij}T, \tag{1}$$

where λ and μ are the Lamé constants, δ_{ij} are the Kronecker-delta components, θ is the volumetric strain, u_i are the displacement components, T is the increment of temperature above a reference absolute temperature T_0, and $\beta = (3\lambda + 2\mu)\alpha$ with α being the coefficient of thermal expansion.

The law of heat conduction is (Carcione *et al.*, 2020)

$$\gamma T_{,ii} = \rho C\dot{T} + \beta T_0\dot{\theta}, \tag{2}$$

where γ is the coefficient of thermal conductivity, ρ is the mass density and C is the specific heat capacity. Equation (2) assumes that the change in temperature is proportional to volume changes, while equation (1) reflects variations in temperature-induced stress.

We apply the following Fourier transform to equations (1) and (2),

$$\bar{u}(\vec{x},\omega) = \int_{-\infty}^{\infty} u(\vec{x},t)e^{-i\omega t}dt, \tag{3}$$

leading to an equation in the $\vec{x}-\omega$ domain (omitting the hat for convenience):

$$\begin{cases} \sigma_{ij} = \lambda\delta_{ij}\theta + \mu u_{i,j} + \mu u_{j,i} - \beta\delta_{ij}T \\ \gamma T_{,ii} = \rho C i\omega T + \beta T_0 i\omega\theta \end{cases}, \tag{4}$$

where ω is the angular frequency. We take the following Fourier transform with respect to $\vec{x}$ to the second equation (4),

$$\bar{T}(\vec{k},\omega) = \iint_{-\infty}^{\infty} T(\vec{x},\omega)e^{-i\vec{k}\cdot\vec{x}}d\vec{x}, \tag{5}$$

resulting in an equation in the $\vec{k}-\omega$ domain:

$$-\gamma k^2\bar{T}(\vec{k},\omega) = \rho C i\omega\bar{T}(\vec{k},\omega) + \beta T_0 i\omega\bar{\theta}(\vec{k},\omega), \tag{6}$$

where k is the magnitude of the wavenumber $\vec{k}$. We obtain the following equation from equation (6)

$$\bar{T}(\vec{k},\omega) = -\frac{\beta T_0 i\omega}{\gamma k^2 + \rho C i\omega}\bar{\theta}(\vec{k},\omega). \tag{7}$$

Applying the 2D inverse Fourier transform to equation (7), we have

$$T(\vec{x},\omega) = \frac{1}{(2\pi)^2}\iint_{-\infty}^{\infty}\bar{T}(\vec{k},\omega)\,e^{i\vec{k}\cdot\vec{x}}d\vec{k} = -\frac{\beta T_0 i\omega}{(2\pi)^2}\iint_{-\infty}^{\infty}\frac{\bar{\theta}(\vec{k},\omega)}{\gamma k^2 + \rho C i\omega}e^{i\vec{k}\cdot\vec{x}}d\vec{k}. \tag{8}$$

On the basis of the convolution theorem, we get

$$T = -\beta T_0 i\omega\theta(\vec{x}) * \frac{1}{(2\pi)^2}\iint_{-\infty}^{\infty}\frac{1}{\gamma k^2 + \rho C i\omega}e^{i\vec{k}\cdot\vec{x}}d\vec{k}. \tag{9}$$

Substituting equation (9) into the first term of equation (4) yields the following thermoelastic boundary condition

$$\sigma_{ij} = \lambda\delta_{ij}\theta + \mu\left(u_{i,j} + u_{j,i}\right) + \beta^2\delta_{ij}T_0 i\omega\theta(\vec{x}) * \frac{1}{(2\pi)^2}\iint_{-\infty}^{\infty}\frac{1}{\gamma k^2 + \rho C i\omega} e^{i\vec{k}\cdot\vec{x}} d\vec{k}. \quad (10)$$

2.2 Aligned thermoelastic crack model

Kawahara (1992) studies the scattering of P and SV waves by a random distribution of aligned open cracks with finite thickness. Guo *et al.* (2018c) further modify the Kawahara model to study P-wave scattering by aligned fluid-saturated cracks. We assume that the stress induced by the temperature fluctuations is negligible in the rock frame compared to that of the pore infill. The scattering of P and SV waves can be formulated on the basis of these aligned fluid-saturated crack models by thermal loading through crack boundaries.

For aligned cracks distributed sparsely, randomly and homogeneously in a 2D elastic medium, the averaging of the wavefield $\vec{u}_{\mathrm{A}}$ at the observation point **A** can be obtained with the Foldy approximation (Foldy, 1945),

$$\langle\vec{u}_{\mathrm{A}}\rangle = \vec{u}_{\mathrm{A}}^0 + \nu \int \vec{S}_{\mathrm{A}}\langle\vec{u}_{ni}\rangle d\vec{r}_{ni}\,, \quad (11)$$

which is the sum of the incident wavefield $\vec{u}_{\mathrm{A}}^0$ and the scattered wavefield. The scattered wavefield $\vec{S}_{\mathrm{A}}\langle\vec{u}_{ni}\rangle$ at the observation point **A** results from averaging of the incident wavefield $\langle\vec{u}_{ni}\rangle$ to the ni-th crack, where $\vec{r}_{ni} = (p_1, p_2)$ denotes the location of the center of this crack. We first consider the incident P wave $\vec{u}_{\mathrm{A}}^0$ in the form

$$\vec{u}_{\mathrm{A}}^0 = A_0 e^{ik_{\mathrm{P}}X_1\sin\varphi + ik_{\mathrm{P}}X_2\cos\varphi}(\sin\varphi, \cos\varphi), \quad (12)$$

where A_0 is the amplitude, the wavenumber k_{P} is defined as ω/v_{P} for the P-wave velocity v_{P} of the background medium, and the time factor $\exp(-i\omega t)$ is omitted for brevity.

We follow Kawahara (1992) to express the averaging $\langle\vec{u}_{\mathrm{A}}\rangle$ of the incident waves at the observation point **A** as

$$\langle \vec{u}_{\mathrm{A}} \rangle = A e^{ik_{\mathrm{P}}X_1 \sin\varphi + ik_{\mathrm{P}}X_2(\cos\varphi + \kappa_{\mathrm{P}}/k_{\mathrm{P}})} \left(\sin\varphi, \cos\varphi + \frac{\kappa_{\mathrm{P}}}{k_{\mathrm{P}}} \right), \tag{13}$$

where A is the amplitude of the unknown average wavefield of the P wave, $\kappa_{\mathrm{P}}/k_{\mathrm{P}}$ is a dimensionless quantity, and κ_{P} is an unknown coefficient describing the P-wave dispersion and attenuation. Appendix A provides a summary to obtain this coefficient for models of scattering by aligned dry cracks, developed by Kawahara (1992).

The thermoelastic boundary condition of fluid saturated cracks becomes

$$\begin{cases} \sigma_{12}^{E} + \sigma_{12}^{S} = 0 \\ \sigma_{22}^{E} + \sigma_{22}^{S} = \lambda_f \theta + \beta_f^2 T_0 i\omega\theta(\vec{x}) * \dfrac{1}{(2\pi)^2} \displaystyle\iint_{-\infty}^{\infty} \frac{1}{\gamma_f k^2 + \rho_f C_f i\omega} e^{i\vec{k}\cdot\vec{x}} d\vec{k} \end{cases}, |x_1| < a, x_2 = 0, \tag{14}$$

where σ_{jk}^{E} and σ_{jk}^{S} are the stress components caused by $\langle \vec{u}_{ni} \rangle$ and $\vec{S}_{nj}\langle \vec{u}_{ni} \rangle$ respectively, $\vec{S}_{nj}\langle \vec{u}_{ni} \rangle$ is the scattered wavefield at the *nj*-th crack by averaging the incident wavefield $\langle \vec{u}_{ni} \rangle$ of the *ni*-th crack, λ_f is the Lamé constant of the fluid, $\beta_f = 3\lambda_f \alpha_f$, with α_f being the thermal expansion coefficient of the fluid, γ_f is the thermal conductivity coefficient of the fluid, ρ_f is the mass density of the fluid, and C_f is the specific heat capacity of the fluid. The fluid applies a pressure and thermal stress on the crack boundary. However, $\theta(\vec{x})$ is difficult to obtain because of the convolution, and we need to simplify the second term of equation (14). Compared to the term $\rho_f C_f i\omega$, the term $\gamma_f k^2$ of the fluid, within the seismic band, in the denominator of equation (14), is very small and can be neglected (see Table 1) and we have

$$\sigma_{ij} = \lambda_f \delta_{ij} \theta + \beta_f^2 \delta_{ij} T_0 \theta(\vec{x}) * \frac{1}{(2\pi)^2} \iint_{-\infty}^{\infty} \frac{1}{\rho_f C_f} e^{i\vec{k}\cdot\vec{x}} d\vec{k}. \tag{15}$$

On the basis of the convolution theorem, we have

$$\sigma_{ij} = \left(\lambda_f + \frac{\beta_f^2 T_0}{\rho_f C_f} \right) \theta \delta_{ij}. \tag{16}$$

Thus, the simplified thermoelastic boundary condition becomes

$$
\begin{cases} \sigma_{12}^{E} + \sigma_{12}^{S} = 0 \\ \sigma_{22}^{E} + \sigma_{22}^{S} = \left(\lambda_f + \dfrac{\beta_f^2 T_0}{\rho_f C_f}\right) \dfrac{[\Delta \vec{u}_{ni}(x_1, p_1, p_2)]_2}{h}, \end{cases} \quad |x_1| < a, x_2 = 0\,, \tag{17}
$$

so that we can model the effective wave dissipation by both scattering and thermoelastic effects. Substituting equations (13) and (A2) into (17) yields

$$
\begin{cases} \displaystyle\int_{-a}^{a} \mathrm{T}_{121}(x_1, 0|\xi_1, 0) D_1(\xi_1)\, d\xi_1 = e^{ik_{\mathrm{P}} x_1 \sin\varphi} \\ \displaystyle\int_{-a}^{a} \mathrm{T}_{222}(x_1, 0|\xi_1, 0) D_2(\xi_1)\, d\xi_1 + \frac{\lambda_f \rho_f C_f + \beta_f^2 T_0}{\rho_f C_f \mu_m h} D_2(x_1) = e^{ik_{\mathrm{P}} x_1 \sin\varphi} \end{cases}, \quad |x_1| < a, \tag{18}
$$

where T_{jkl} is given in Appendix B, and D_j is given in equation (A5). We adopt Yamashita's (1990) method to solve for D_j numerically, and equation (18) is transformed into the following form

$$
\begin{cases} \displaystyle\int_{-1}^{1} \hat{T}_{121}(s, 0|\hat{\xi}_1, 0) \hat{D}_1(\hat{\xi}_1)\, d\hat{\xi}_1 = e^{i\hat{k}_{\mathrm{P}} s \sin\varphi} \\ \displaystyle\int_{-1}^{1} \hat{T}_{222}(s, 0|\hat{\xi}_1, 0) \hat{D}_2(\hat{\xi}_1)\, d\hat{\xi}_1 + \frac{\lambda_f \rho_f C_f + \beta_f^2 T_0}{\rho_f C_f \mu_m h} \hat{D}_2(s) = e^{i\hat{k}_{\mathrm{P}} s \sin\varphi} \end{cases}, \quad |s| < 1\,, \tag{19}
$$

which is discretized as

$$
\begin{cases} \displaystyle\sum_{n=1}^{M-1} T_{mn}^{121} \hat{D}_{1n} = e^{i\hat{k}_{\mathrm{P}} s_m \sin\varphi} \\ \displaystyle\sum_{n=1}^{M-1} \left(T_{mn}^{222} + \frac{\lambda_f \rho_f C_f + \beta_f^2 T_0}{\rho_f C_f \mu_m h} \delta_{mn} \right) \hat{D}_{2n} = e^{i\hat{k}_{\mathrm{P}} s_m \sin\varphi} \end{cases}, \quad m = 1, \ldots, M-1, \tag{20}
$$

where $\hat{D}$ is assumed to be approximately constant in the *n*-th interval, $s_m = -1 + m\Delta s$, $\Delta s = 2/M$, M is the discretization number,

$$
\begin{cases} \hat{\xi}_1 = \dfrac{\xi_1}{a}, s = \dfrac{x_1}{a}, \hat{k}_{\mathrm{P}} = a k_{\mathrm{P}} \\ \hat{T}_{j2j} = a^2 \mathrm{T}_{j2j}, \hat{D}_j = \dfrac{D_j}{a}, j = 1,2 \end{cases},
$$

and $T_{mn}^{j2j} = \int_{s_n - \Delta s/2}^{s_n + \Delta s/2} \hat{T}_{j2j}(s_m, 0|\hat{\xi}_1, 0) d\hat{\xi}_1 \quad (j = 1,2)$.

We can obtain $\hat{D}_j$ $(j = 1,2)$ from equation (20), $[\Delta \vec{u}_{ni}]_j$ $(j = 1,2)$ can be represented by equation (A5) and then we can obtain $[\vec{S}_{nj}\langle\vec{u}_{ni}\rangle]_j$. Substituting $[\vec{S}_{nj}\langle\vec{u}_{ni}\rangle]_j$ and equation (12) into equation (11), and using equation (13), yields

$$\kappa_{\mathrm{P}} = \nu k_{\mathrm{P}} a^2 \left[\hat{\phi}_1 f \sin 2\varphi \sin\varphi + \frac{\hat{\phi}_2}{2f\cos\varphi}(1-2f\sin^2\varphi)^2\right], \tag{21}$$

where $f = v_{\mathrm{SV}}^2/v_{\mathrm{P}}^2$, with v_{SV} being the SV-wave velocity of the background medium or rock frame, $\hat{\phi}_j = \sum_{m=1}^{M-1}\hat{D}_{jm}e^{-i\hat{k}_{\mathrm{P}}s_m\sin\varphi}\Delta s$ $(j = 1,2)$. The phase velocity V_{P} and attenuation factor Q_{P}^{-1} of the P wave can be obtained as (Kawahara and Yamashita, 1992)

$$\begin{cases} V_{\mathrm{P}} = \left(1 - \mathrm{Re}\kappa_{\mathrm{P}}\dfrac{\cos\varphi}{k_{\mathrm{P}}}\right)v_{\mathrm{P}} \\ Q_{\mathrm{P}}^{-1} = 2\mathrm{Im}\kappa_{\mathrm{P}}\dfrac{\cos\varphi}{k_{\mathrm{P}}} \end{cases}, \tag{22}$$

where Re and Im represent the real and imaginary parts, respectively.

For the incident SV wave, we consider

$$\vec{u}_{\mathrm{A}}^0 = B_0 e^{ik_{\mathrm{SV}}X_1\sin\phi + ik_{\mathrm{SV}}X_2\cos\phi}(\cos\phi, -\sin\phi), \tag{23}$$

where B_0 is the amplitude, and the wavenumber k_{SV} is defined as ω/v_{SV}. The averaging $\langle\vec{u}_{\mathrm{A}}\rangle$ of this wave at the observation point **A** can be expressed as

$$\langle\vec{u}_{\mathrm{A}}\rangle = Be^{ik_{\mathrm{SV}}X_1\sin\phi + ik_{\mathrm{SV}}X_2(\cos\phi + \kappa_{\mathrm{SV}}/k_{\mathrm{SV}})}\left(\cos\phi + \frac{\kappa_{\mathrm{SV}}}{k_{\mathrm{SV}}}, -\sin\phi\right), \tag{24}$$

where B is the amplitude of the unknown average wavefield, and κ_{SV} is the unknown coefficient describing the SV-wave dispersion and attenuation.

Similar to κ_{P}, we have

$$\kappa_{\mathrm{SV}} = \nu k_{\mathrm{SV}} a^2 \left[\hat{\phi}_1 \frac{\cos^2 2\phi}{2\cos\phi} + \hat{\phi}_2 \sin 2\phi \sin\phi\right]. \tag{25}$$

The phase velocity V_{SV} and attenuation factor Q_{SV}^{-1} of the SV wave can be obtained as (Kawahara and Yamashita, 1992)

$$\begin{cases} V_{\mathrm{SV}} = \left(1 - \mathrm{Re}\kappa_{\mathrm{SV}}\dfrac{\cos\phi}{k_{\mathrm{SV}}}\right)v_{\mathrm{SV}} \\ Q_{\mathrm{SV}}^{-1} = 2\mathrm{Im}\kappa_{\mathrm{SV}}\dfrac{\cos\phi}{k_{\mathrm{SV}}} \end{cases}. \tag{26}$$

3 Examples

The frequency-dependent response as a function of temperature, is calculated for various incidence angles. To highlight the thermoelastic effect, we compare the scattering dispersion and attenuation between the thermoelastic and conventional boundary conditions, where the latter has been implemented by Guo *et al.* (2018c). The former is related to the displacement discontinuities across the cracks and associated with the effect of temperatures through the fluid inside a crack.

We consider the following number density, length, and thickness of the cracks: 2.5×10^{-5} m^{-2}, 40 m, and 0.4 m, respectively. The material properties for the background medium at 10 MPa pressure are given by Simmons and Brace (1965) as: $\lambda_m = 19$ GPa, $\mu_m = 40.4$ GPa, and $\rho_m = 2650$ $\mathrm{kg/m^3}$. The physical properties are assumed to be constant within a certain temperature range. The fluid (water) properties at 10 MPa are given in Kretzschmar and Wagner (2019), as listed in Table 1.

Figure 2 shows the dissipation factor and phase velocity due to the P-wave scattering as a function of frequency at $\varphi = 0°$ incidence for the three different temperatures. The behavior can be classified into three stages: i) low-frequency Rayleigh scattering, with increasing attenuation and slightly decreasing velocity, ii) middle-frequency Mie scattering dominated by strong attenuation and rapidly increasing velocity, and iii) high-frequency scattering with decreasing attenuation but almost constant velocity. We see that the attenuation and dispersion become strong with increasing temperature, which are dominated by the Rayleigh and Mie scatterings, whereas the high-frequency thermoelastic effect on the scattering is negligible. The behavior is similar for both the thermoelastic and conventional boundary conditions. However, there are differences in magnitude at different temperatures, due to the thermal-stress effect, which weakens the scattering attenuation and dispersion because of the reduction in stiffness contrast across the cracks. Due to the variation of the interference pattern between the scattered wavefields originated from the crack tips (Kawahara and Yamashita, 1992), there are some periodic fluctuations in the high frequency domain. Figures 3 and 4 show the same quantities of Figure 2, but at the 45° and 90° incidence angles, respectively. We see that the scattering dispersion and attenuation for both boundary conditions are weaker compared to normal incidence, since the cracks are difficult to compress because effects related to the Poisson ratio. However, changes in magnitude induced by temperature differences can be identified at low and medium frequencies. The thermoelastic effect at large incidence angles is negligible, because the thermal stress caused by the temperature fluctuations is weak compared to small incidence angles.

Figure 5 displays the same quantities of Figure 2, but for the SV wave at $\phi = 0°$ incidence. The dispersion and attenuation curves do not depend on temperatures for both boundary conditions, because the shear modulus in fluid-saturated cracks is zero, and the polarization direction of the SV wave is orthogonal to the propagation direction. In summary, since temperature fluctuations do not cause shear stress, both boundary conditions result in the same dispersion and attenuation. Figures 6 and 7 show the same quantities of Figure 5, but at the 45° and 90° incidence angles, respectively. As for the P wave, the SV wave dispersion and attenuation for both boundary conditions decrease with increasing incidence angle. Unlike the case of normal incidence, shown in Figure 5, the properties vary with temperature. In contrast to the P wave, the dispersion and attenuation variations of the SV wave are more pronounced as a function of the incidence angle. Similarly, the thermoelastic effect on the dissipation is weaker than that of the conventional boundary condition, because of an additional thermal stress imposed by the thermoelastic boundary condition on the crack boundaries.

Figure 8 shows the P-wave dissipation factor and phase velocity as a function of temperature at $\varphi = 0°$ and three different frequencies, corresponding to Rayleigh, Mie and high-frequency scattering, respectively. For both boundary conditions, attenuation and dispersion are stronger at intermediate frequencies and high temperatures. However, the thermoelastic effect reduce the anelastic effects. Figure 9 displays the same quantities of Figure 8, but for the SV wave and $\phi = 90°$, where the same effects can be observed.

4 Conclusions

We have developed an isothermal thermoelastic model coupling the elastic deformation of cracks with thermal effects. By combining the thermoelastic theory with the representation theorem of non-interaction Foldy approximation, we model the dispersion and attenuation of P and SV waves induced by aligned fluid-saturated cracks constrained by a thermoelastic boundary condition. The examples analyze the frequency-dependent response for various incidence angles and temperatures by comparison to the conventional crack model. The results indicate the dissipation increases with increasing temperature, but weakens the scattering effect at a given temperature due to the influence of the thermal stress. The P wave shows a strong sensitivity to temperature along the direction perpendicular to the cracks because of the anisotropic nature of the aligned crack system, while the SV wave behaves in opposite manner. The model may have some potential to evaluate the temperature distribution from seismic attributes. Future investigations include the generalization of the theory to a non-isothermal background medium.

Appendix A

Based on the representation theorem (e.g., Wickham, 1981)

$$\left[\vec{S}_{nj}\langle\vec{u}_{ni}\rangle\right]_j = -\int_{-a}^{a}[\Delta\vec{u}_{ni}(\xi_1,p_1,p_2)]_l\,\Gamma_{jl}(x_1,x_2|\xi_1,0)d\xi_1,\qquad j,l=1,2, \tag{A1}$$

where $\left[\vec{S}_{nj}\langle\vec{u}_{ni}\rangle\right]_j$ is the j-th component of the scattered wavefield $\vec{S}_{nj}\langle\vec{u}_{ni}\rangle$ at the nj-th crack by averaging the incident wavefield $\langle\vec{u}_{ni}\rangle$ of the ni-th crack, $[\Delta\vec{u}_{ni}(\xi_1,p_1,p_2)]_l$ is the l-th component of the displacement discontinuity across the ni-th crack, and the Green function stress tensor Γ_{jl} is

$$\Gamma_{jl}(x_1,x_2|\xi_1,\xi_2) = \frac{i}{4}\left[\delta_{l2}\left(1-2\frac{k_{\mathrm{P}}^2}{k_{\mathrm{SV}}^2}\right)\frac{\partial}{\partial x_j}H_0^{(1)}(k_{\mathrm{P}}R) + \left(\delta_{jl}\frac{\partial}{\partial x_2}+\delta_{j2}\frac{\partial}{\partial x_l}\right)H_0^{(1)}(k_{\mathrm{SV}}R)\right.$$
$$\left. -\frac{2}{k_{\mathrm{SV}}^2}\frac{\partial^3}{\partial x_j\partial x_l\partial x_2}\left(H_0^{(1)}(k_{\mathrm{P}}R)-H_0^{(1)}(k_{\mathrm{SV}}R)\right)\right],\qquad j,l=1,2,$$

where $k_{\mathrm{SV}}=\omega/v_{\mathrm{SV}}$ is the wavenumber, with v_{SV} being the SV-wave velocity of the background medium, $R=\sqrt{(x_1-\xi_1)^2+(x_2-\xi_2)^2}$, and $H_0^{(1)}(kR)$ denotes the zero-order Hankel function of the first kind. The stress induced by $\langle\vec{u}_{ni}\rangle$ and $\vec{S}_{nj}\langle\vec{u}_{ni}\rangle$ can be written as (Kawahara and Yamashita, 1992; Guo *et al.*, 2018c)

$$\begin{cases}\sigma_{jk}^E = \lambda_m\delta_{jk}\frac{\partial}{\partial x_l}[\langle\vec{u}_{ni}\rangle]_l + \mu_m\left(\frac{\partial}{\partial x_k}[\langle\vec{u}_{ni}\rangle]_j+\frac{\partial}{\partial x_j}[\langle\vec{u}_{ni}\rangle]_k\right)\\ \sigma_{jk}^S = -\mu_m\int_{-a}^{a}[\Delta\vec{u}_{ni}(\xi_1,p_1,p_2)]_l\,T_{jkl}(x_1,x_2|\xi_1,0)d\xi_1\end{cases},\quad j,k,l=1,2, \tag{A2}$$

from Hooke’s law and equation (A1), where λ_m and μ_m are the Lamé constants of the background medium and T_{jkl} is given in Appendix B.

The boundary condition of the dry cracks is

$$\sigma_{12}^{E}+\sigma_{12}^{S}=\sigma_{22}^{E}+\sigma_{22}^{S}=0, \qquad |x_1|<a, x_2=0. \tag{A3}$$

Substituting equations (13) and (A2) into (A3) yields

$$\int_{-a}^{a} \mathrm{T}_{j2j}(x_1,0|\xi_1,0) D_j(\xi_1)\, d\xi_1 = e^{ik_{\mathrm{P}}x_1\sin\varphi}, \qquad |x_1|<a, j=1,2, \tag{A4}$$

where

$$\begin{cases} D_1(\xi_1)=\dfrac{[\Delta\vec{u}_{ni}(\xi_1,p_1,p_2)]_1}{2i(k_{\mathrm{P}}\cos\varphi+\kappa_{\mathrm{P}})\sin\varphi A e^{ik_{\mathrm{P}}p_1\sin\varphi+ik_{\mathrm{P}}p_2(\cos\varphi+\kappa_{\mathrm{P}}/k_{\mathrm{P}})}} \\ D_2(\xi_1)=\dfrac{[\Delta\vec{u}_{ni}(\xi_1,p_1,p_2)]_2}{ik_{\mathrm{P}}Ae^{ik_{\mathrm{P}}p_1\sin\varphi+ik_{\mathrm{P}}p_2(\cos\varphi+\kappa_{\mathrm{P}}/k_{\mathrm{P}})}\left[\left(\frac{k_{\mathrm{SV}}^2}{k_{\mathrm{P}}^2}-2\right)\sin^2\varphi+\frac{k_{\mathrm{SV}}^2}{k_{\mathrm{P}}^2}\left(\cos\varphi+\frac{\kappa_{\mathrm{P}}}{k_{\mathrm{P}}}\right)^2\right]} \end{cases}. \tag{A5}$$

The following expression for κ_{P} can be obtained (Kawahara, 1992; Guo *et al.*, 2018c)

$$\kappa_{\mathrm{P}}=\nu\phi_1 f k_{\mathrm{P}}\sin2\varphi\sin\varphi+\nu\phi_2\frac{k_{\mathrm{P}}}{2f\cos\varphi}(1-2f\sin^2\varphi)^2, \tag{A6}$$

where $f=v_{\mathrm{SV}}^2/v_{\mathrm{P}}^2$ and $\phi_j(k_{\mathrm{P}},\varphi)=\int_{-a}^{a}D_j(\xi_1)e^{-ik_{\mathrm{P}}\xi_1\sin\varphi}\,d\xi_1$ $(j=1,2)$.

Appendix B

Expressions of T_{jkl} are given in Kawahara and Yamashita's paper (1992), as

$$T_{jkl}(x_1,x_2|\xi_1,\xi_2)=T_{jkl}^{*}(x_1,x_2|\xi_1,\xi_2)$$

$$+\frac{i}{4}\left[\left(\delta_{jl}\frac{\partial^2}{\partial x_k\partial x_2}+\delta_{k2}\frac{\partial^2}{\partial x_j\partial x_l}+\delta_{kl}\frac{\partial^2}{\partial x_j\partial x_2}+\delta_{j2}\frac{\partial^2}{\partial x_k\partial x_l}\right)H_0^{(1)}(k_{\mathrm{SV}}R)\right.$$

$$-\frac{4}{k_{\mathrm{SV}}^2}\frac{\partial^4}{\partial x_j\partial x_k\partial x_l\partial x_2}\left(H_0^{(1)}(k_{\mathrm{P}}R)\right.$$

$$\left.\left.-H_0^{(1)}(k_{\mathrm{SV}}R)\right)\right], \tag{B1}$$

$$T_{111}^{*}(x_1,x_2|\xi_1,\xi_2)=\frac{i}{2}\left(1-2\frac{k_{\mathrm{P}}^2}{k_{\mathrm{SV}}^2}\right)\frac{\partial^2}{\partial x_1\partial x_2}H_0^{(1)}(k_{\mathrm{P}}R)=T_{122}^{*}(x_1,x_2|\xi_1,\xi_2)$$

$$=T_{212}^{*}(x_1,x_2|\xi_1,\xi_2)$$

$$=T_{221}^{*}(x_1,x_2|\xi_1,\xi_2), \tag{B2}$$

$$T_{112}^{*}(x_1,x_2|\xi_1,\xi_2)$$

$$=\frac{i}{4}\frac{k_{\mathrm{SV}}^2}{k_{\mathrm{P}}^2}\left(1-2\frac{k_{\mathrm{P}}^2}{k_{\mathrm{SV}}^2}\right)\left(\frac{\partial^2}{\partial x_1^2}\right.$$

$$\left.+\frac{\partial^2}{\partial x_2^2}\right)H_0^{(1)}(k_{\mathrm{P}}R), \tag{B3}$$

$$T_{121}^{*}(x_1,x_2|\xi_1,\xi_2)=T_{211}^{*}(x_1,x_2|\xi_1,\xi_2)$$

$$=0, \tag{B4}$$

$$T_{222}^{*}(x_1,x_2|\xi_1,\xi_2)$$

$$=\frac{i}{4}\frac{k_{\mathrm{SV}}^2}{k_{\mathrm{P}}^2}\left[\left(1-2\frac{k_{\mathrm{P}}^2}{k_{\mathrm{SV}}^2}\right)^2\frac{\partial^2}{\partial x_1^2}\right.$$

$$\left.+\left(1-4\frac{k_{\mathrm{P}}^4}{k_{\mathrm{SV}}^4}\right)\frac{\partial^2}{\partial x_2^2}\right]H_0^{(1)}(k_{\mathrm{P}}R). \tag{B5}$$

Acknowledgements

The research was supported by the National Natural Science Foundation of China (grant no. 41720104006, 41821002), and 111 Project "Deep-Superdeep Oil & Gas Geophysical Exploration" (B18055). No experimental data are used in this paper.

References

Aki, K. (1980). Attenuation of shear-waves in the lithosphere for frequencies from 0.05 to 25 Hz, *Physics of the Earth and Planetary Interiors*, 21(1), 50-60.

Armstrong, B. H. (1984). Models for thermoelastic attenuation of waves in heterogeneous solids, *Geophysics*, 49, 1032-1040.

Biot, M. A. (1956). Thermoelasticity and irreversible thermodynamics, *Journal of Applied Physics*, 27, 240-253.

Boschi, E. (1973). A thermoviscoelastic model of the earthquake source mechanism, *Journal of Geophysical Research*, 78, 7733-7737.

Carcione, J. M., Cavallini, F., Wang, E., Ba, J., & Fu, L.Y. (2019). Physics and simulation of wave propagation in linear thermo-poroelastic media, *Journal of Geophysical Research*, 124(8), 8147-8166.

Carcione, J. M., Wang, Z. W., Ling, W., Salusti, E., Ba, J., & Fu, L.Y. (2018). Simulation of wave propagation in linear thermoelastic media, *Geophysics*, 84, T1-T11.

Carcione, J. M., Gei, D., Santos, J. E., Fu, L. Y., & Ba, J. (2020). Canonical analytical solutions of wave-induced thermoelastic attenuation, *Geophysical Journal International*, 221(2), 835-842.

Cermak, V., Bodri, L., Rybach, L., & Buntebarth, G. (1990). Relationship between seismic velocity and heat production: comparison of two sets of data and test of validity, *Earth and Planetary Science Letters*, 99(1-2), 48-57.

Deresiewicz, H. (1957). Plane waves in a thermoelastic solid, *Journal of the Acoustical Society of America*, 29, 204-209.

Eslami, M. R., Hetnarski, R. B., Ignaczak, J., Noda, N., Sumi, N., & Tanigawa, Y. (2013). *Theory of elasticity and thermal stresses* (Vol. 197, p. 786), Dordrecht: Springer.

Foldy, L. L. (1945). The multiple scattering of waves. I. General theory of isotropic scattering by randomly distributed scatters, *Physical Review*, 67(3-4), 107.

Fu, B. Y., Guo, J., Fu, L. Y., Glubokovskikh, S., Galvin, R. J., & Gurevich, B. (2018). Seismic dispersion and attenuation in saturated porous rock with aligned slit cracks, *Journal of Geophysical Research: Solid Earth*, 123(8), 6890-6910.

Fu, B. Y., Fu, L. Y., Guo, J., Galvin, R. J., & Gurevich, B. (2020). Semi-analytical solution to the problem of frequency dependent anisotropy of porous media with an aligned set of slit cracks, *International Journal of Engineering Science*, 147, 103209.

Fu, L. Y. (2012). Evaluation of sweet spot and geopressure in Xihu, Sag. Tech Report, CCL2012-SHPS-0018ADM. Key laboratory of petroleum resource research, Institute of Geology and Geophysics, Chinese Academy of Sciences.

Fu, L. Y. (2017). Deep-superdeep oil gas geophysical exploration 111. Program report jointly initiated by MOE and SAFEA, B18055. School of Geosciences China University of Petroleum (East China).

Galvin, R. J., & Gurevich, B. (2006). Interaction of an elastic wave with a circular crack in a fluid-saturated porous medium, *Applied Physics Letters*, 88(6), 061918.

Galvin, R. J., & Gurevich, B. (2007). Scattering of a longitudinal wave by a circular crack in a fluid-saturated porous medium, *International Journal of Solids and Structures*, 44(22-23), 7389-7398.

Galvin, R. J., & Gurevich, B. (2009). Effective properties of a poroelastic medium containing a distribution of aligned cracks, *Journal of Geophysical Research: Solid Earth*, 114(B7).

Green, A. E., & Lindsay, K. A. (1972). Thermoelasticity, *Journal of elasticity*, 2, 1-7.

Guo, J., Germán Rubino, J., Barbosa, N. D., Glubokovskikh, S., & Gurevich, B. (2018a). Seismic dispersion and attenuation in saturated porous rocks with aligned farctures of finite thickness: Theory and numerical simulations—Part 1: P-wave perpendicular to the crack plane, *Geophysics*, 83(1), WA49-WA62.

Guo, J., Germán Rubino, J., Barbosa, N. D., Glubokovskikh, S., & Gurevich, B. (2018b). Seismic dispersion and attenuation in saturated porous rocks with aligned fractures of finite thickness: Theory and numerical simulations—Part 2: Frequency-dependent anisotropy, *Geophysics*, 83(1), WA63-WA71.

Guo, J., Shuai, D., Wei, J., Ding, P., & Gurevich, B. (2018c). P-wave dispersion and attenuation due to scattering by aligned fluid saturated fractures with finite thickness: theory and experiment, *Geophysical Journal International*, 215(3), 2114-2133.

Jacquey, A. B., Cacace, M., Blöcher, G., & Scheck-Wenderoth, M. (2015). Numerical investigation of thermoelastic effects on fault slip tendency during injection and production of geothermal fluids, *Energy Procedia*, 76, 311-320.

Kawahara, J. (1992). Scattering of P, SV waves by random distribution of aligned open cracks, *Journal of Physics of the Earth*, 40(3), 517-524.

Kawahara, J. & Yamashita, T. (1992). Scattering of elastic waves by a fracture zone containing randomly distributed cracks, *Pure and applied geophysics*, 139(1), 121-144.

Kikuchi, M. (1981). Dispersion and attenuation of elastic waves due to multiple scattering from cracks, *Physics of the Earth and Planetary Interiors*, 27(2), 100-105.

Krenk, S., & Schmidt, H. (1982). Elastic wave scattering by a circular crack, Philosophical Transactions of the Royal Society of London. Series A, *Mathematical and Physical Sciences*, 308(1502), 167-198.

Kretzschmar, H. J., & Wagner, W. (2019). International Steam Tables: Properties of Water and Steam Based on the Industrial Formulation IAPWS-IF97. Springer.

Lord, H. W., & Shulman, Y. (1967). A generalized dynamical theory of thermoelasticity, *Journal of the Mechanics and Physics of Solids*, 15, 299-309.

Mal, A. K. (1970a). Interaction of elastic waves with a penny-shaped crack, *International Journal of Engineering Science*, 8(5), 381-388.

Mal, A. K. (1970b). Interaction of elastic waves with a Griffith crack, *International Journal of Engineering Science*, 8(9), 763-776.

Martin, P. A. (1981). Diffraction of elastic waves by a penny-shaped crack. Proceedings of the Royal Society of London. A. *Mathematical and Physical Sciences*, 378(1773), 263-285.

Phurkhao, P. (2013). Compressional waves in fluid-saturated porous solid containing a penny-shaped crack, *International Journal of Solids and Structures*, 50(25-26), 4292-4304.

Poletto, F., Farina, B., & Carcione, J. M. (2018). Sensitivity of seismic properties to temperature variations in a geothermal reservoir, *Geothermics*, 76, 149-163.

Ritsema, J., Deuss, A. A., Van Heijst, H. J., & Woodhouse, J. H. (2011). S40RTS: a degree-40 shear-velocity model for the mantle from new Rayleigh wave dispersion, teleseismic traveltime and normal-mode splitting function measurements, *Geophysical Journal International*, 184(3), 1223-1236.

Rudgers, A. J. (1990). Analysis of thermoacoustic wave propagation in elastic media, *Journal of the Acoustical Society of America*, 88, 1078-1094.

Sato, H., Fehler, M. C., & Maeda, T. (2012). Seismic wave propagation and scattering in the heterogeneous earth: Second Edition, Springer.

Savage, J. (1966). Thermoelastic attenuation of elastic waves by cracks, *Journal of Geophysical Research*, 71, 3929–3938.

Simmons, G., & Brace, W. F. (1965). Comparison of static and dynamic measurements of compressibility of rocks. *Journal of Geophysical Research*, 70(22), 5649-5656.

Simmons, N. A., Forte, A. M., Boschi, L., & Grand, S. P. (2010). GyPSuM: A joint tomographic model of mantle density and seismic wave speeds, *Journal of Geophysical Research: Solid Earth*, 115(B12).

Song, Y., Hu, H., & Rudnicki, J. W. (2017). Normal compression wave scattering by a permeable crack in a fluid-saturated poroelastic solid, *Acta Mechanica Sinica*, 33(2), 356-367.

Song, Y., Hu, H., & Han, B. (2019). Elastic wave scattering by a fluid-saturated circular crack and effective properties of a solid with a sparse distribution of aligned cracks, *The Journal of the Acoustical Society of America*, 146(1), 470-485.

Song, Y., Hu, H., & Han, B. (2020a). Seismic attenuation and dispersion in a cracked porous medium: An effective medium model based on poroelastic linear slip conditions, *Mechanics of Materials*, 140, 103229.

Song, Y., Hu, H., & Han, B. (2020b). Effective properties of a porous medium with aligned cracks containing compressible fluid, *Geophysical Journal International*, 221(1), 60-76.

Treitel, S. (1959). On the Attenuation of Small-Amplitude Plane Stress Waves in a Thermoelastic Solid, *Journal of Geophysical Research*, 64, 661-665.

Wang, Z. W., Fu, L. Y., Wei, J., Hou, W., Ba, J., & Carcione, J. M. (2019). On the Green function of the Lord–Shulman thermoelasticity equations, *Geophysical Journal International*, 220(1), 393-403.

Wei, J., Fu, L. Y., Wang, Z. W., Ba, J., & Carcione, J. M. (2020). Green function of the Lord-Shulman thermo-poroelasticity theory, *Geophysical Journal International*, 221, 1765–1776.

Wickham, G. R. (1981). The diffraction of stress waves by a plane finite crack in two dimensions: uniqueness and existence. *Proceedings of the Royal Society of London. A. Mathematical and Physical Sciences*, 378(1773), 241-261.

Yamashita, T. (1990). Attenuation and dispersion of SH waves due to scattering by randomly distributed cracks, *Pure and applied geophysics*, 132, 545–568.

Zhang, C.H. & Achenbach, J. D. (1991). Effective wave velocity and attenuation in a material with distributed penny-shaped cracks, *International journal of solids and structures*, 27(6), 751-767.

Zhang, C.H. & Gross, D. (1993a). Wave attenuation and dispersion in randomly cracked solids—I. Slit cracks, *International journal of engineering science*, 31(6), 841-858.

Zhang, C.H. & Gross, D. (1993b). Wave attenuation and dispersion in randomly cracked solids—II. Penny-shaped cracks, *International journal of engineering science*, 31(6), 859-872.

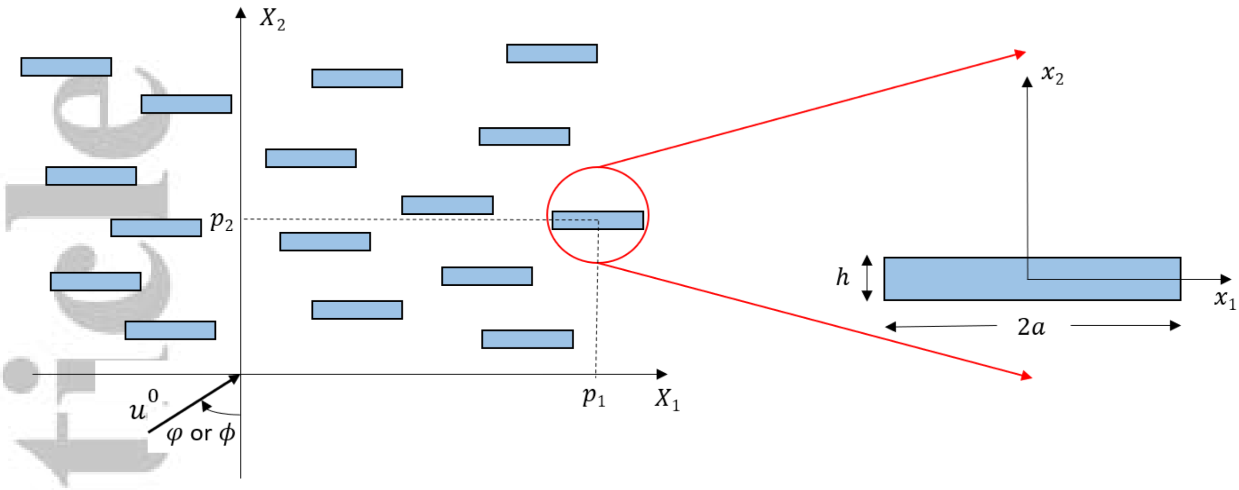

Figure 1. Aligned fluid-saturated cracks of thickness h and length $2a$, distributed sparsely, randomly and homogeneously in an infinite, isothermal, and isotropic elastic background medium. The cracks are assumed to be parallel to the X_1-axis but infinitely long along the X_3-axis, to satisfy the plane-strain condition in the X_1–X_2 plane. The origin of the local coordinate system (x_1, x_2) is fixed at the center of the *ni*-th crack with a global coordinate (p_1, p_2). u^0 represents the harmonic plane incident P (or SV) wave at an angle φ (or ϕ) with respect to the X_2-axis. The model is modified from Kawahara (1992) and Guo *et al.* (2018c).

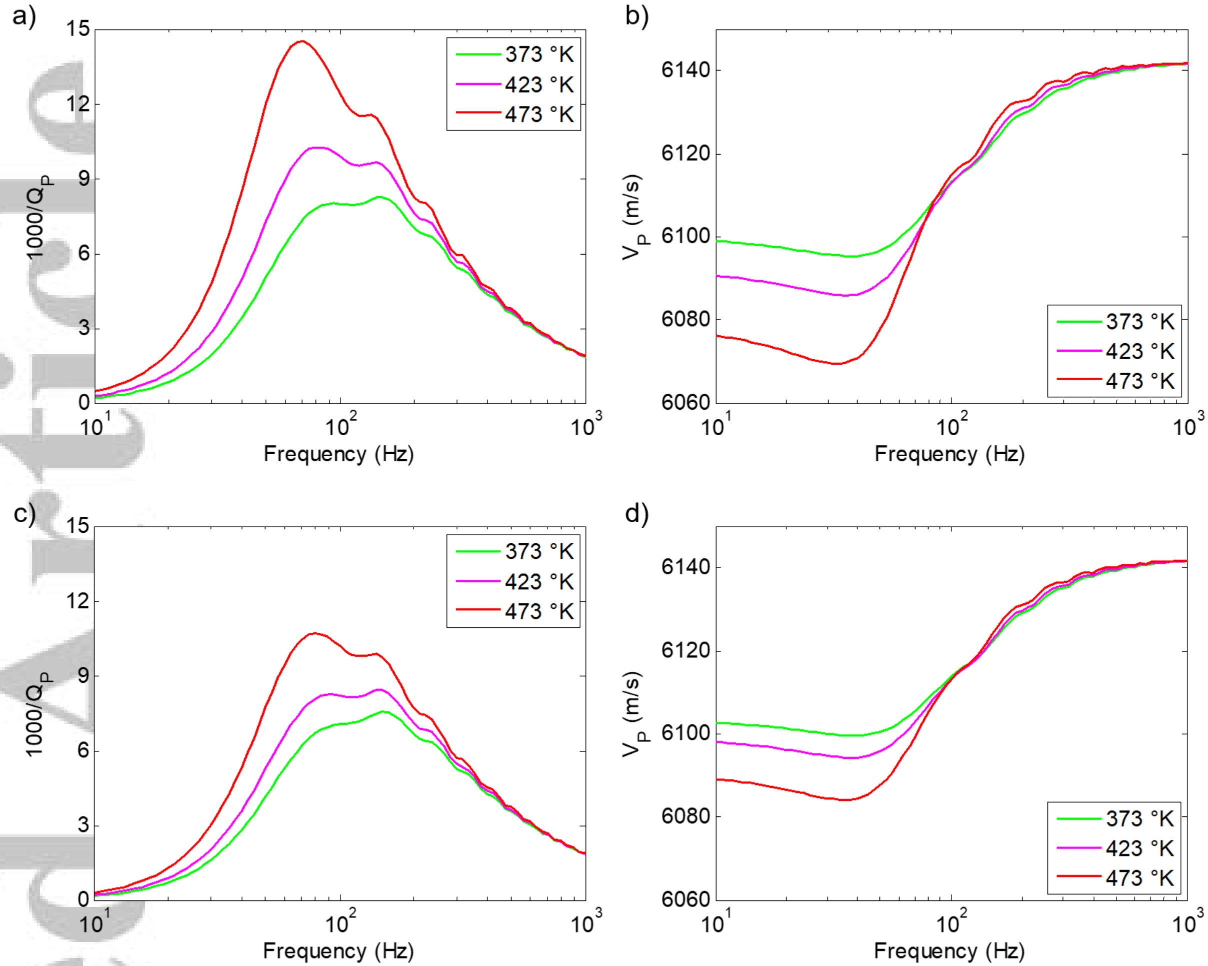

Figure 2. Dissipation factor and phase velocity of the P-wave scattering as a function of frequency at $\varphi = 0°$ and three different temperatures; (a and b): conventional boundary condition and (c and d): thermoelastic boundary condition.

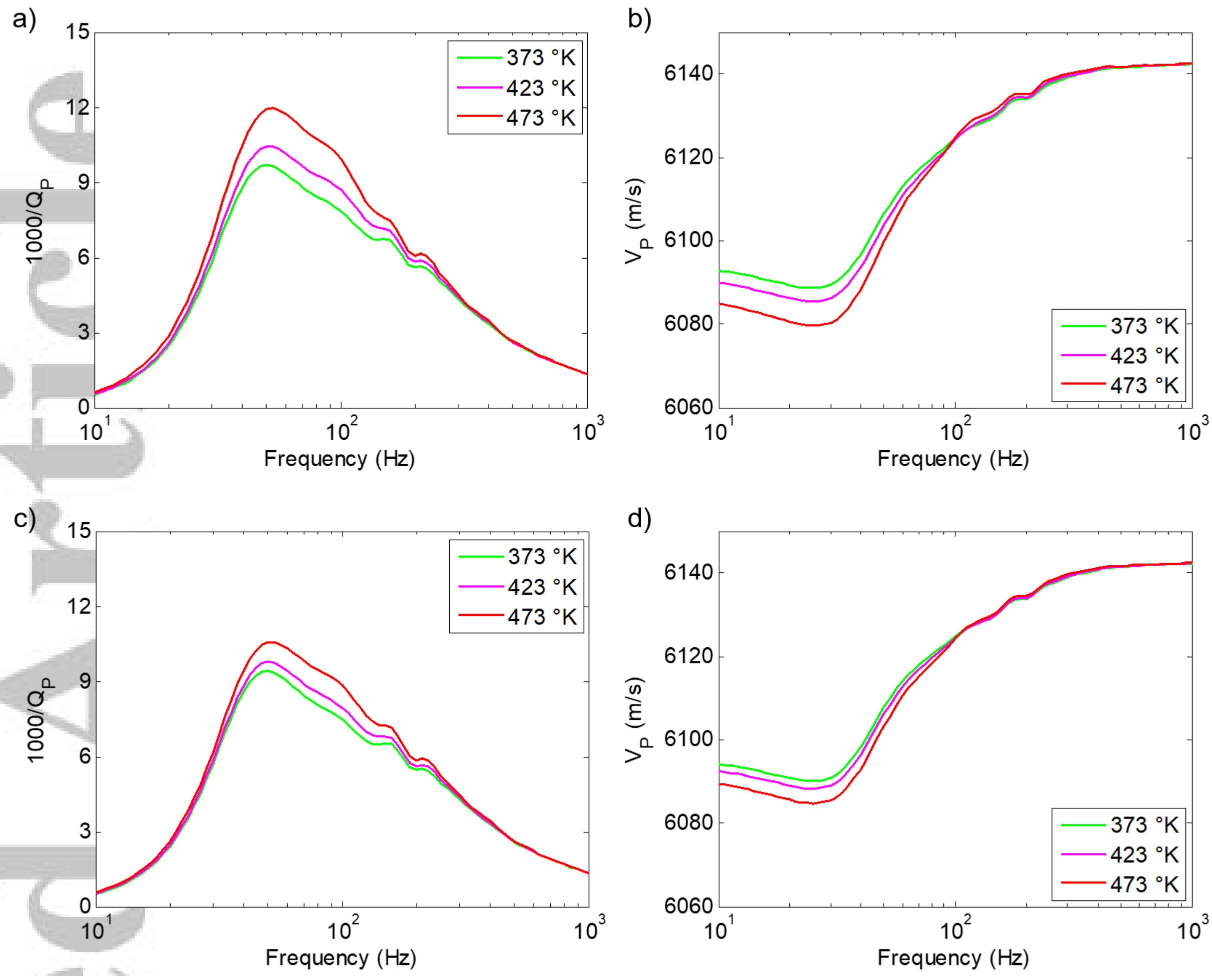

Figure 3. Same as Figure 2, but at $\varphi = 45°$.

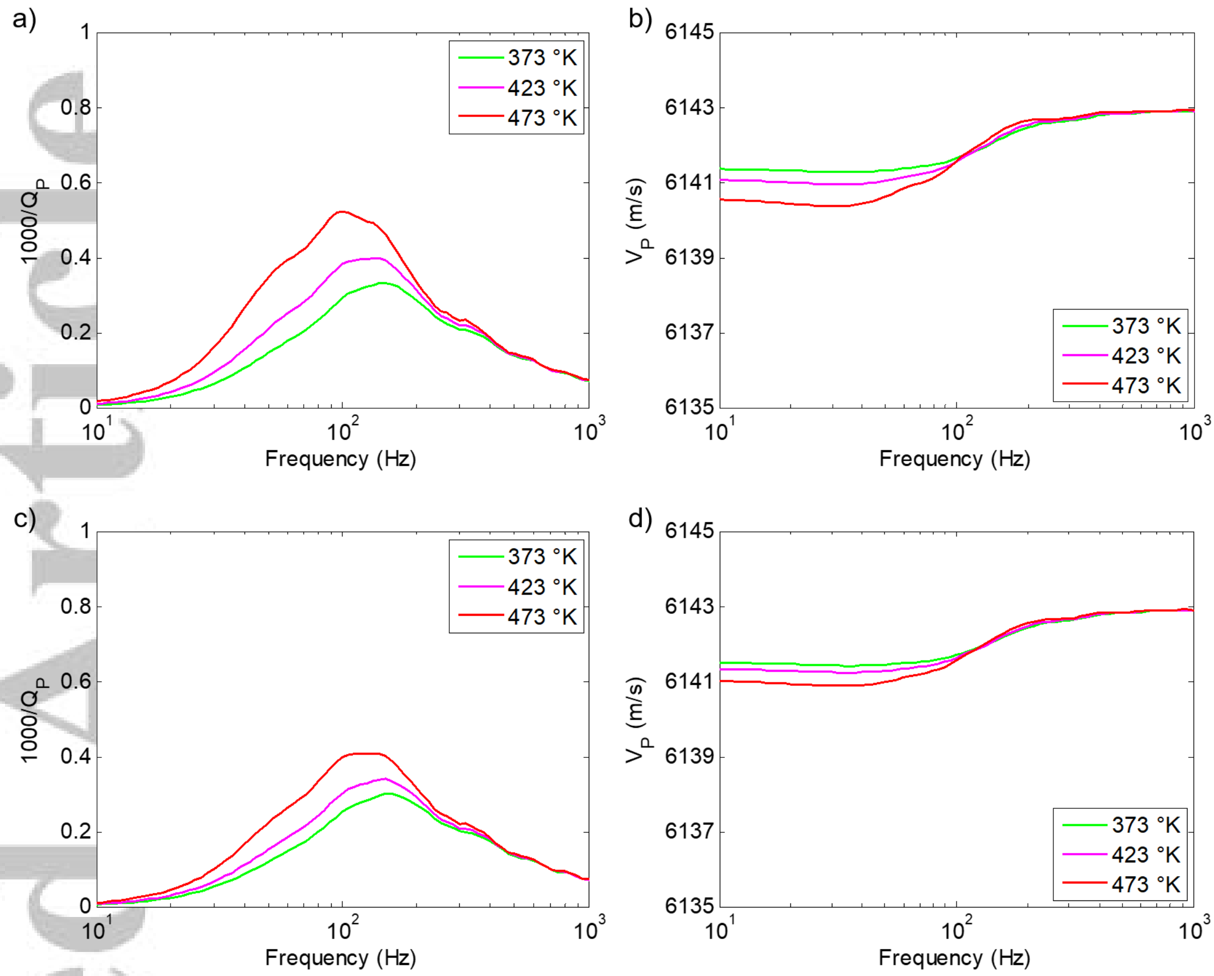

Figure 4. Same as Figure 2, but at $\varphi = 90°$.

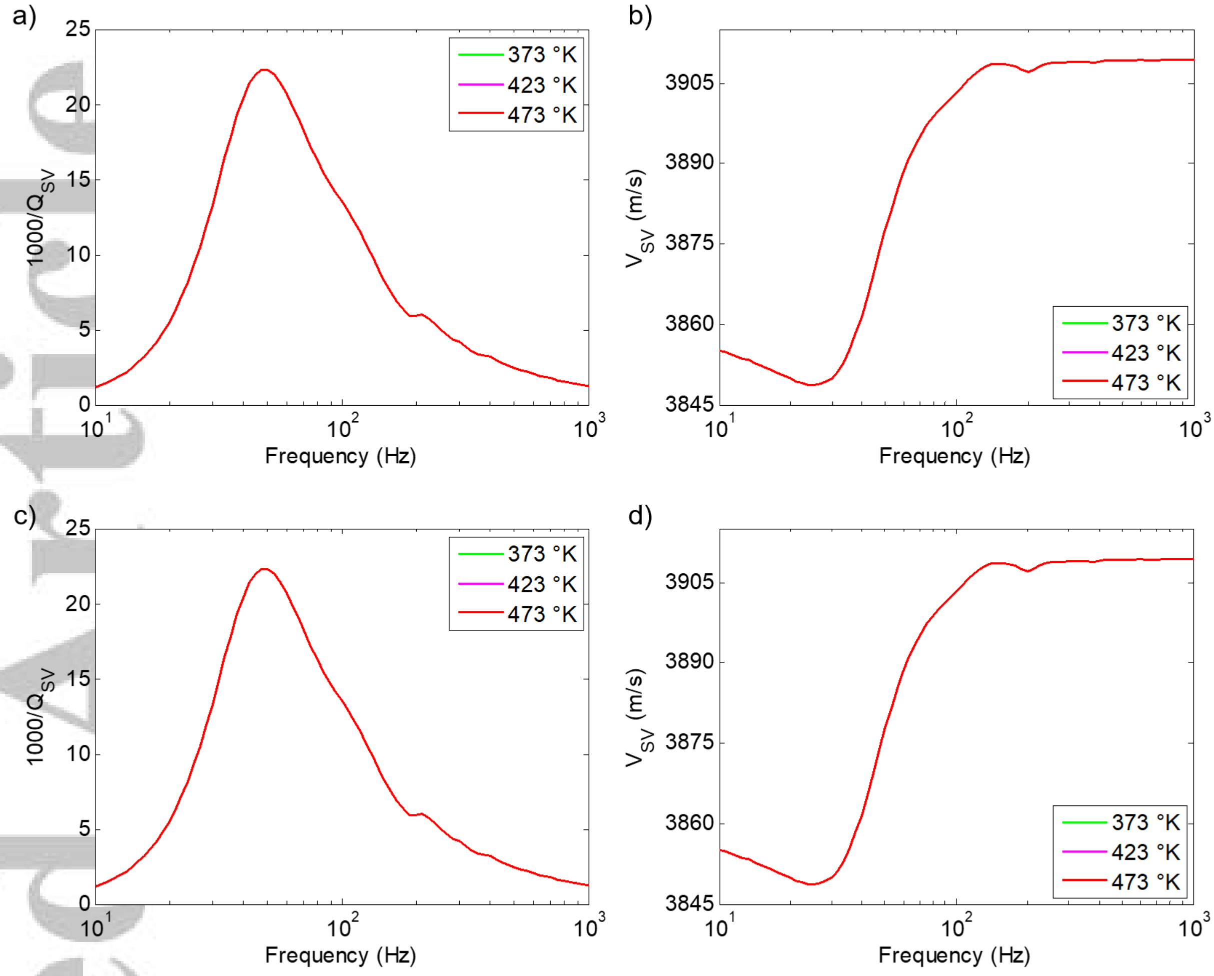

Figure 5. Same as Figure 2, but for the SV wave at $\phi = 0°$.

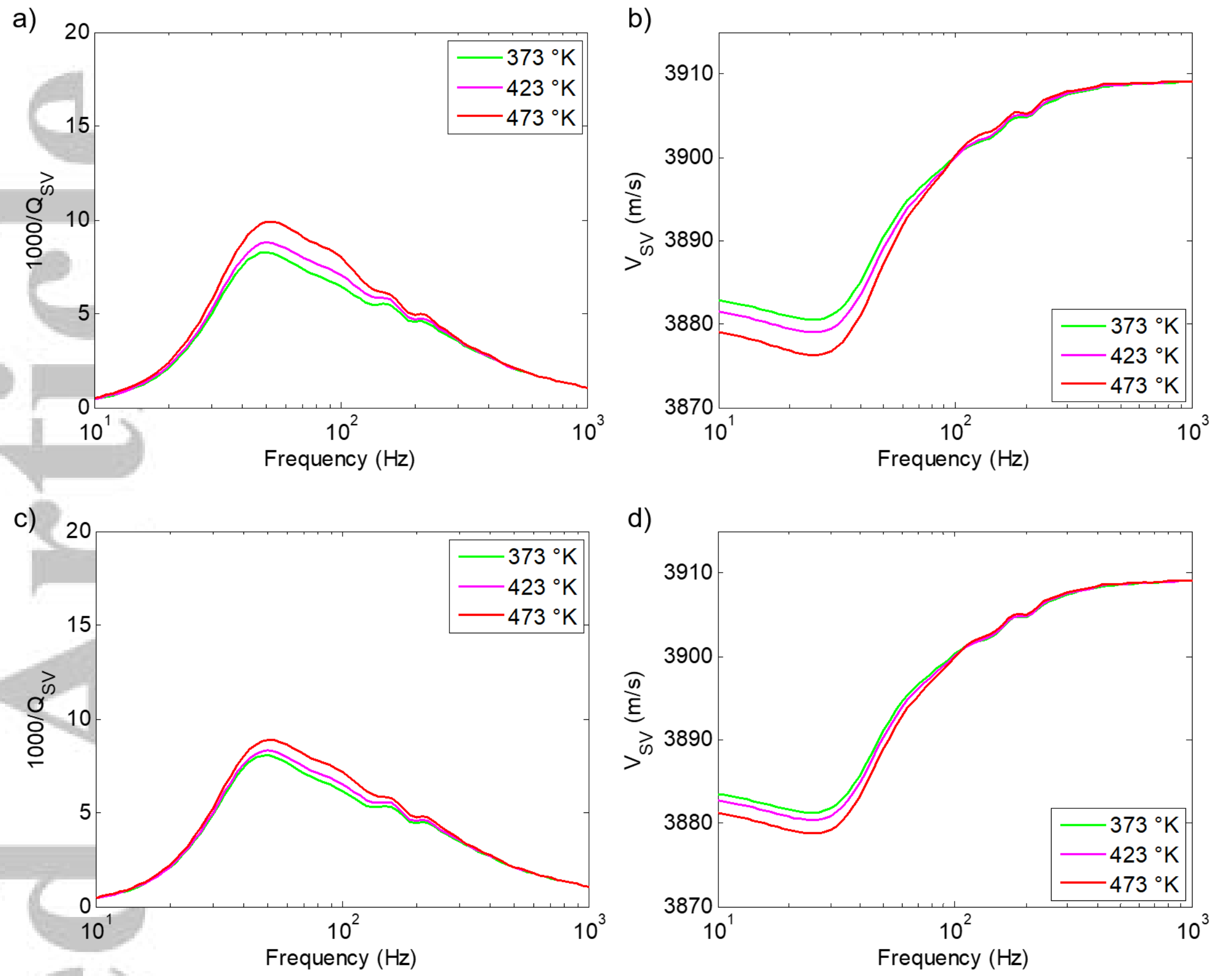

Figure 6. Same as Figure 5, but at $\phi = 45°$.

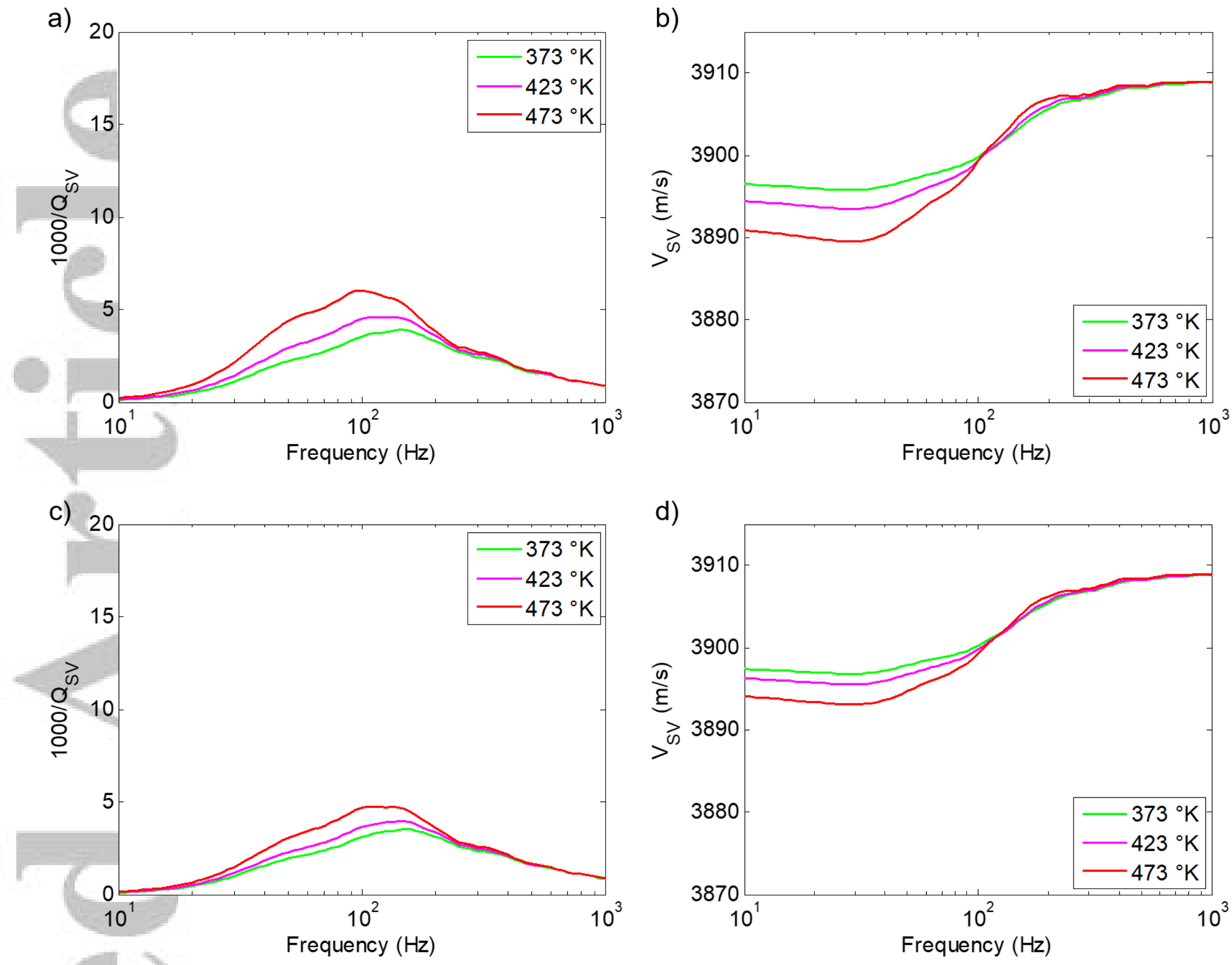

Figure 7. Same as Figure 5, but at $\phi = 90°$.

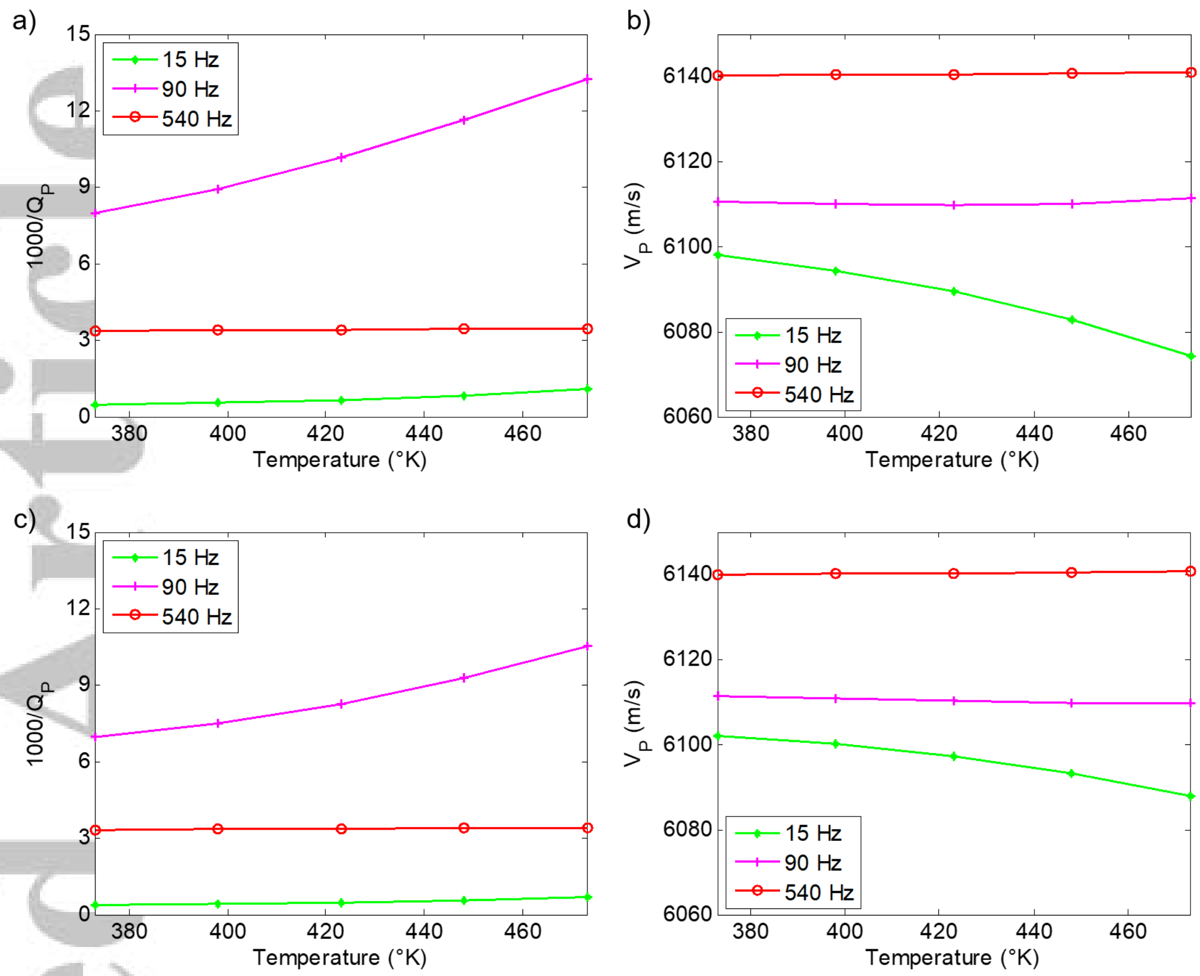

Figure 8. Dissipation factor and phase velocity due to P-wave scattering as a function of temperature at $\varphi = 0°$ and three different frequencies; (a and b): conventional boundary condition, and (c and d): thermoelastic boundary condition.

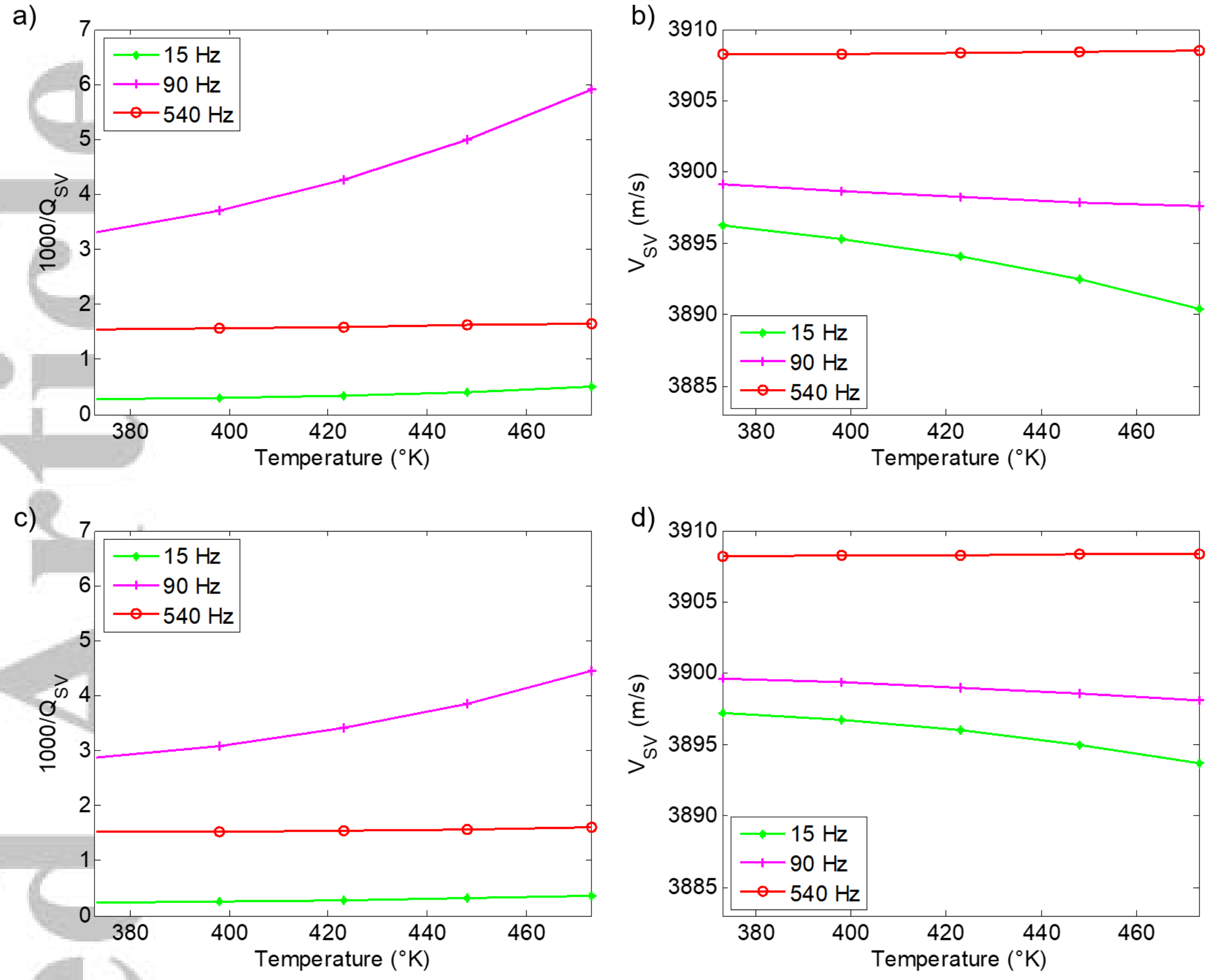

Figure 9. Same as Figure 8, but for the SV wave at $\phi = 90°$.

Table 1. Water properties at five temperatures and 10 MPa.

T_0	α_f	ρ_f	C_f	λ_f	γ_f
°K	10^{-6}/°K	kg/m^3	m^2/(s^2 · °K)	MPa	m · kg/(s^3 · °K)
373	260.5	962.9	4194.5	2110.8	0.684
398	312.0	943.9	4230.3	1911.9	0.689
423	367.9	922.3	4280.6	1685.5	0.688
448	432.9	898.1	4350.1	1446.0	0.682
473	513.3	870.9	4447.2	1203.3	0.671